

## Estimation of velocity change using repeating earthquakes with different locations and focal mechanisms

Chinaemerem O. Kanu,<sup>1</sup> Roel Snieder,<sup>1</sup> and Dan O'Connell<sup>2</sup>

Received 28 September 2012; revised 29 April 2013; accepted 30 April 2013; published 14 June 2013.

[1] Coda of repeating earthquakes carry information about the time-lapse changes in the subsurface or reservoirs. Some of the changes within a reservoir change the seismic velocity, and thereby, the seismic signals that travel through the reservoir. We investigate, both theoretically and numerically, the impact of the perturbations in seismic source properties of used repeating earthquakes on time-lapse velocity estimation. We derive a criterion for selecting seismic events that can be used in velocity analysis. This criterion depends on the dominant frequency of the signals, the centertime of the used time window in a signal, and the estimated relative velocity change. The criterion provides a consistent framework for monitoring changes in subsurface velocities using microseismic events and the ability to assess the accuracy of the velocity estimations.

**Citation:** Kanu, C. O., R. Snieder, and D. O'Connell (2013), Estimation of velocity change using repeating earthquakes with different locations and focal mechanisms, *J. Geophys. Res. Solid Earth*, 118, 2905–2914, doi:10.1002/jgrb.50206.

### 1. Introduction

[2] Monitoring temporal changes within the Earth's subsurface is a topic of interest in many areas of geophysics. These changes can result from an earthquake and its associated change in stress [Cheng *et al.*, 2010], fluid injection or hydrofracturing [Davis *et al.*, 2003], and oil and gas production [Zoback and Zinke, 2002]. Some of the subsurface perturbations induced by these processes include temporal and spatial velocity changes, stress perturbations, changes in anisotropic properties of the subsurface, and fluid migration. Many of these changes span over a broad period of time and might even influence tectonic processes, such as induced seismicity [Zoback and Harjes, 1997]. For example, Kilauea, Hawaii (which erupted in November 1975) is suggested to have triggered a magnitude 7.2 earthquake within a half hour of the eruption [Lipman *et al.*, 1985]. A seismic velocity perturbation of the subsurface leads to progressive time shifts across the recorded seismic signals. Various methods and data have been used to resolve the velocity perturbations. These methods include seismic coda wave interferometry [Snieder *et al.*, 2002], doublet analysis of repeating microseismic and earthquake codas [Poupinet *et al.*, 1984], time-lapse tomography [Vesnaver *et al.*, 2003], and ambient seismic noise analysis [Cheng *et al.*, 2010; Sens-Schönfelder and Wegler, 2006; Wegler and Sens-Schönfelder, 2007; Brenguier *et al.*, 2008; Meier

*et al.*, 2010]. Earthquake codas have higher sensitivity to the changes in the subsurface because multiple scattering allows these signals to sample the area of interest multiple times. However, there are inherent challenges in the use of these signals. Doublet analysis of the earthquake (microseismic) codas requires repeating events. Failure to satisfy the requirement that the events are identical can compromise the accuracy of the estimated velocity changes. In this study, we focus on the estimation of velocity changes using codas of repeating earthquakes that are not quite identical in their locations and source mechanisms.

[3] Fluid-triggered microseismic events often are repeatable but in practice events occur at slightly different positions with somewhat different source mechanisms [Sasaki and Kaieda, 2002; Miyazawa *et al.*, 2007; Godano *et al.*, 2012]. Changes in the source properties might result from coseismic stress changes [Asano *et al.*, 2011] or changes in the properties of the event rupture locations [McGuire *et al.*, 2012]. Imprints of the source perturbation and the velocity change on the seismic waveforms can be subtle. Therefore, we will need to ask, how do the source location, source mechanism, and subsurface perturbations affect the estimated velocity changes? Snieder [2006] shows that we can retrieve velocity changes from the coda of the waveforms recorded prior to and after the change. Robinson *et al.* [2011] develop a formulation using coda wave interferometry to estimate changes in source parameters of double-couple sources from correlation of the coda waves of doublets. Snieder and Vrijlandt [2005], using a similar formulation, relate the shift in the source location to the variance of the traveltimes perturbations between the doublet signals. In all these studies, the authors assume that the expected (average) change in traveltimes of the coda (due to either changes in the source locations or source mechanisms) is zero.

[4] In this study, we investigate the impact of changes in source properties on the estimation of relative velocity

<sup>1</sup>Center for Wave Phenomena, Colorado School of Mines, Golden, Colorado, USA.

<sup>2</sup>Fugro Consultants, Inc., William Lettis and Associates Division, Lakewood, Colorado, USA.

Corresponding author: C. O. Kanu, Geophysics Department, Colorado School of Mines, 1500 Illinois Street, Golden, CO 80401-1887, USA. (ckanu@mines.edu)

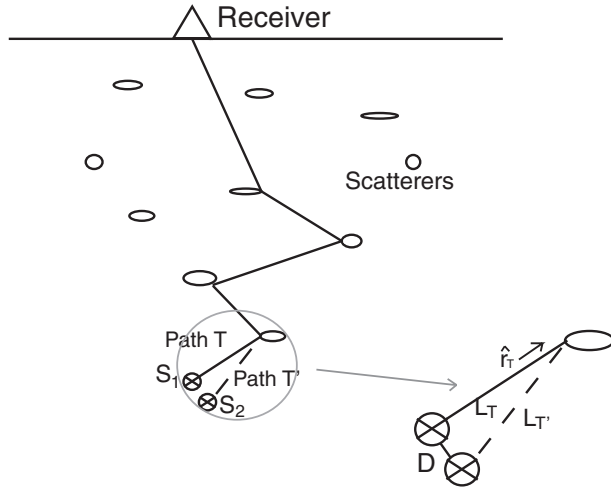


**Figure 1.** Geometry of wave paths. Source,  $S_1$ , produces the unperturbed signal while Source,  $S_2$ , produces the perturbed signal. Path  $T$  shows the scattering path for the unperturbed signal, and the scattering path for the perturbed signal is defined by Path  $T'$ . The sources are separated by a distance  $D$ , and the source distances are  $L_T$  and  $L_{T'}$  distance away from the first scatterer along path  $T$  and  $T'$ , respectively. The unit vector  $\hat{r}_T$  defines the direction traveled by the signal before the signal first encounters a scatterer.

changes. Knowledge of the impact of these perturbations on the estimated velocity change allows for a consistent framework for selecting pairs of earthquakes or microearthquakes used for analyzing the velocity changes. This results in a more robust estimation of velocity change. In section 2, we explore the theoretical relationships between the velocity changes and perturbations in the earthquake source properties. Following this section is a numerical validation of the theoretical results. We explain the implications and limitations of our results in section 4. In the appendices, we explain the mathematical foundation of our results in this study.

## 2. Mathematical Consideration

[5] In this section, we use the time-shifted cross correlation [Snieder, 2002, 2006] to develop an expression for the average value of the time perturbation of scattered waves that are excited by sources with varying source properties. This perturbation is due to changes in the velocity of the subsurface and to changes in the source properties. These changes, we assume, may occur concurrently. Figure 1 is a schematic figure showing the general setup of the problem we are investigating. Two sources ( $S_1$  and  $S_2$ ) represent a doublet (repeating seismic events). These events occur at different locations and may have different rupture patterns. We assume that these events can be described by a double couple. We investigate the ability of using the signals of these sources for time-lapse monitoring of velocity changes, assuming that these sources occur at different times. We express the signals of the two sources as unperturbed and perturbed signals, where the perturbation refers to any change in the signal due to changes within the subsurface and/or the source properties.

[6] The unperturbed seismic signal  $U(t)$  is given as

$$U(t) = A \sum_T U^{(T)}(t), \quad (1)$$

and the perturbed seismic signal  $\hat{U}(t)$  is given as

$$\hat{U}(t) = \hat{A} \sum_T (1 + \zeta^{(T)}) U^{(T)}(t - t_p^T), \quad (2)$$

where  $A$  and  $\hat{A}$  are the amplitudes of the unperturbed and perturbed source signals, respectively. These amplitudes represent the strengths of the sources. The recorded waves are a superposition of wave propagation along all travel paths as denoted by the summation over paths  $T$ . The change in the source focal mechanism only affects the amplitude of the wave traveling along each trajectory  $T$  because the excitation of waves by a double couple is real [Aki and Richards, 2002]. The change in the signal amplitudes—due to changes in the source mechanism angles—is defined by  $\zeta^{(T)}$  for path  $T$ , and  $t_p^T$  is the time shift on the unperturbed signal due to the medium perturbation for path  $T$ . The change in the signal amplitudes along path  $T$  depends on the source radiation angles. In this study, we assume that the medium perturbation results from the velocity change within the subsurface and changes in the source properties. The time-shifted cross correlation of the two signals is given as

$$C(t_s) = \int_{t-t_w}^{t+t_w} U(t') \hat{U}(t' + t_s) dt', \quad (3)$$

where  $t$  is the centertime of the employed time window and  $2t_w$  is the window length. The normalized time-shifted cross

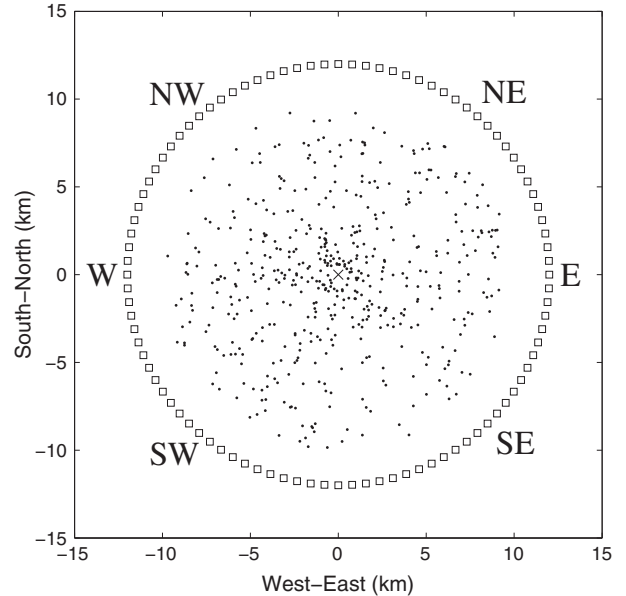


**Figure 2.** The experiment geometry of the numerical simulation. The receivers (squares) are surrounding the point scatterers (black dots). The source is positioned in the origin (cross). All perturbations of the source location is done from this position. The stations marked (NW, NE, E, SE, and SW) are used in the presentation of results in Figures 7 and 8.

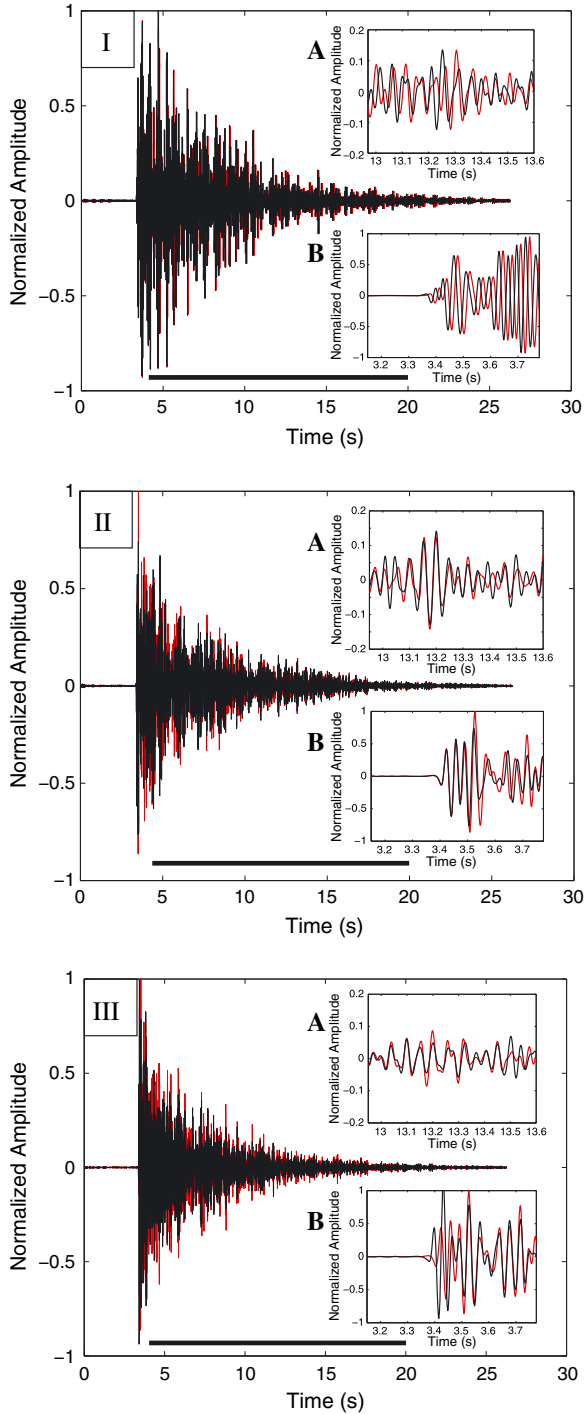


**Figure 3.** Recorded seismic signals at station E (Figure 2), the reference signal (red line), and (I) the time-lapse signal (black line) with 0.4% relative velocity change, (II) the time-lapse signal (black line) with  $0.14\lambda_d$  source displacement, and (III) the time-lapse signal (black line) with  $20^\circ$  source angle perturbations. Inset A shows the late coda while inset B shows the first arrivals of the two signals. The black bold line is the time window used for data processing. Time 0 is the source rupture time.

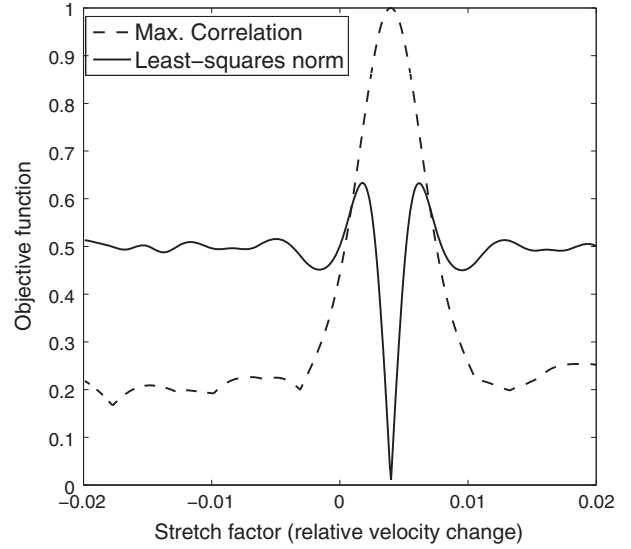


**Figure 4.** The objective function  $R(\epsilon)$  (solid line) as a function of the stretch factor  $\epsilon$ . The objective function is minimum for  $\epsilon = 0.4\%$ , which corresponds to the time velocity change. The corresponding maximum correlation of the stretch factors is given by the dashed lines.

correlation  $R(t_s)$  can be expressed as follows:

$$R(t_s) = \frac{\int_{t-t_w}^{t+t_w} U(t') \hat{U}(t' + t_s) dt'}{\left( \int_{t-t_w}^{t+t_w} U^2(t') dt' \int_{t-t_w+t_s}^{t+t_w+t_s} \hat{U}^2(t') dt' \right)^{\frac{1}{2}}}. \quad (4)$$

The time-shifted cross correlation has a maximum at a time lag equal to the average time perturbation ( $t_s = \langle t_p \rangle$ ) of all waves that arrive in the used time window [Snieder, 2006]:

$$\left. \frac{\partial C(t_s)}{\partial t_s} \right|_{(t_s = \langle t_p \rangle)} = 0. \quad (5)$$

Equation (5) allows for the extraction of the average traveltimes perturbation from the cross correlation. In this study, the average of a quantity  $f$  is a normalized intensity weighted sum of the quantity [Snieder, 2006]:

$$\langle f \rangle = \frac{\sum_T A_T^2 f_T}{\sum_T A_T^2}, \quad (6)$$

where  $A_T^2 = \int (U^T(t'))^2 dt'$  is the intensity of the wave that has propagated along path  $T$ .

[7] We show in sections A and B that the expected value of the time perturbation and its variance are given by

$$\langle t_p \rangle = - \left\langle \frac{\delta V}{V_0} \right\rangle t \quad (7)$$

and

$$\sigma_t^2 = \langle t_p^2 \rangle - \langle t_p \rangle^2 \simeq \frac{D^2}{3V_0^2}. \quad (8)$$

In the above equations,  $\langle \delta V/V_0 \rangle$  is the average relative velocity change,  $D$  is the shift in the source location, and  $V_0$  is the unperturbed velocity of a wave mode. This result is applicable to any wave mode. Equation (7) suggests that the average time shift in the multiple scattered signals depends only on

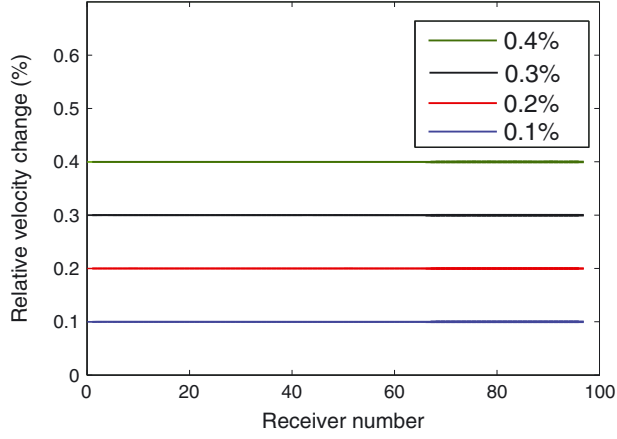


**Figure 5.** Estimated relative velocity change for model velocity change of  $\langle \frac{\delta V}{V_0} \rangle = 0.1\%$  (blue),  $\langle \frac{\delta V}{V_0} \rangle = 0.2\%$  (red),  $\langle \frac{\delta V}{V_0} \rangle = 0.3\%$  (black), and  $\langle \frac{\delta V}{V_0} \rangle = 0.4\%$  (green). The receiver numbers are counted counter-clockwise from the W station in Figure 2.

the velocity changes within the subsurface. The variance of the time shifts depends, however, on the perturbations of the source location.

### 3. Numerical Validation

#### 3.1. Description of Numerical Experiments

[8] We test the equations in section 2 with a numerical simulation using Foldy's multiply scattering theory [Foldy, 1945] described by Groenenboom and Snieder [1995]. The theory models multiple scattering of waves by isotropic point scatterers. We conduct our numerical experiments using a circular 2-D geometry (Figure 2) with point scatterers surrounded by 96 receiver stations. We uniformly assign the imaginary component of the scattering amplitude  $ImA = -4$  to all the scatterers. In 2-D, this is the maximum scattering strength that is consistent with the optical theorem that accounts for conservation of energy [Groenenboom and Snieder, 1995]. The wave radiated by the earthquakes is modulated by the far-field  $P$ -wave radiation pattern  $F^P$ :

$$U_0(\mathbf{r}) = F^P G^{(0)}(\mathbf{r}, \mathbf{r}_s), \quad (9)$$

where  $G^{(0)}(\mathbf{r}, \mathbf{r}_s)$  is the Green's function between the source location  $\mathbf{r}_s$  and any other point  $\mathbf{r}$ . In 2-D, where the takeoff direction is restricted within the 2-D plane,  $F^P$  is given as [Aki and Richards, 2002]

$$F^P = \cos \lambda \sin \delta \sin 2(\psi - \phi) - \sin \lambda \sin 2\delta \sin^2(\psi - \phi), \quad (10)$$

where  $\psi$  is the azimuth of the outgoing wave and  $\lambda$ ,  $\delta$ , and  $\phi$  are the source parameters (rake, dip, and strike, respectively). Sources are located at the center of the scattering area. The source spectrum has a dominant frequency  $f_d$  of approximately 30 Hz and a frequency range of 10–50 Hz. The source spectrum tapers off at the frequency extremes by a cosine taper with a length given by half of the bandwidth. We assume a reference velocity  $V_0 = 3500$  m/s. Because the model we are using is an isotropic multiple scattering

model, the transport mean free path is the same as the scattering mean free path:  $l^* = l$ . The scattering mean free path  $l^*$  [Busch et al., 1994; Groenenboom and Snieder, 1995] is given by

$$l^* = \frac{k_o}{\rho |ImA|}, \quad (11)$$

where  $k_o$  is the wave number of the scattered signal and  $\rho$  is the scatterer density. For our model, the mean free path  $l^*$  is approximately 30.5 km. There is no intrinsic attenuation in the numerical model.

[9] We generate multiple scattered signals, which are recorded at the receivers, using the numerical model in Figure 2. These signals are generated with a reference model defined by the following reference parameter values: the source radiation parameters  $\phi = 0^\circ$ ,  $\lambda = 0^\circ$ , and  $\delta = 90^\circ$ ; change in medium velocity  $\Delta V = 0$  m/s; and shift in the source location  $D = 0$  m. We refer to signals generated by this reference model as the reference signals. In order to understand the effect of the perturbation of these parameters on velocity change estimation, we also generate synthetic signals from the perturbed version of the model. The perturbed model consists of perturbation of either the source locations, source radiation parameters, the medium velocity, or a combination of these. Synthetic signals from the reference and the 0.4% velocity perturbed models are shown in Figure 3a with zoom insets showing the stretching of the waveform by the velocity perturbation. The result of the velocity perturbation on the signals is a progressive time

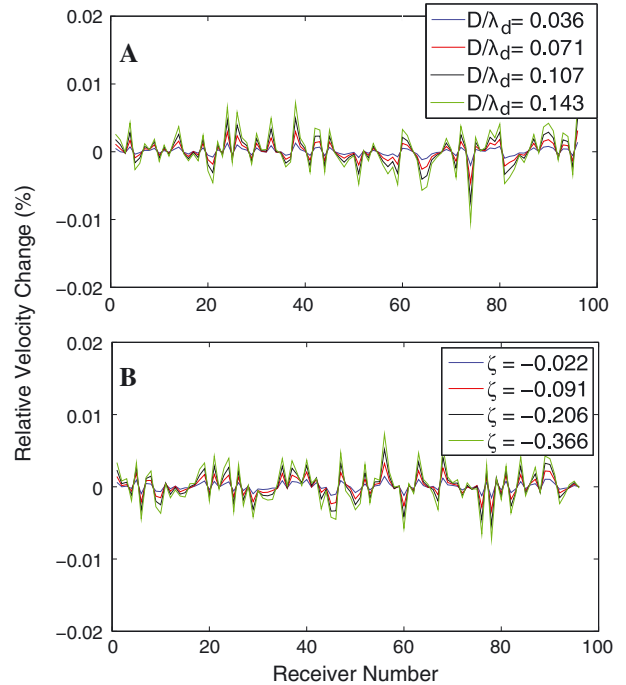


**Figure 6.** Estimated relative velocity change due to perturbation in the source location and the source radiation. (a) The estimated velocity change for perturbed source location (divided by the dominant wavelength; inset in the top right) and (b) the estimated velocity change caused by changes in source radiation angles (inset in the top right). The value of  $\zeta$  is given by equation (14). The receiver numbers are counted counter-clockwise from the W station in Figure 2.

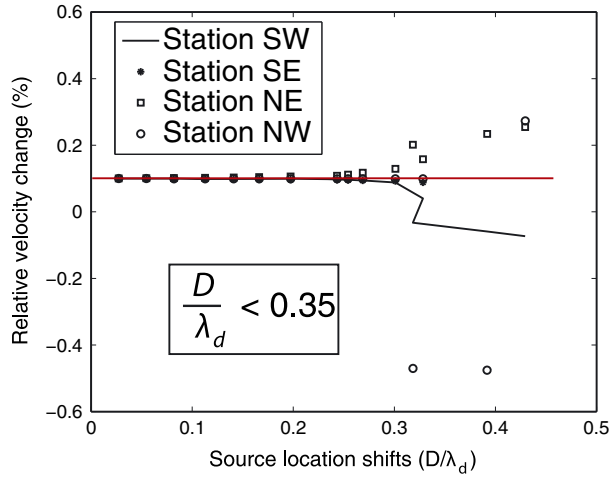


**Figure 7.** Estimated relative velocity change after a 0.1% velocity change and various source location perturbations (Table 1). The shift in the source locations are divided by the dominant wavelength  $\lambda_d$  of the recorded signals. For values of the source location shift greater than  $\lambda_d/4$ , we have incorrect estimates for the velocity change due to the distortion of the perturbed signal. Stations SW, SE, NE, and NW positions are given in Figure 2. The red line indicates the model (accurate) velocity change.

shift of the arriving seismic phases in the signals. Similarly, the effect of the independent perturbation of the source locations and the source radiation parameters are shown in Figures 3b and 3c, respectively. The source location perturbation is  $0.14\lambda_d$  along the  $z$  direction, and the source radiation perturbation is  $20^\circ$  for both the strike, rake, and dip angles. The zoom insets in these Figures 3b and 3c show that the changes in the source properties result in amplitude differences between the time-lapse signals. There are also phase differences between the time-lapse signals due to the perturbation of the source locations.

### 3.2. Data Processing

[10] To estimate the velocity perturbations or possible velocity change imprints on the synthetic signals due to the perturbation of the source location or its radiation properties, we use the stretching algorithm of *Hadziioannou et al.* [2009] who demonstrate the stability and robustness of the algorithm relative to the moving time-window cross correlation of *Snieder et al.* [2002] and the moving time-window cross-spectral analysis of *Poupinet et al.* [1984]. Both algorithms satisfy the relative velocity change equation [*Snieder, 2006*]:

$$\left\langle \frac{t_p}{t} \right\rangle = -\epsilon, \quad (12)$$

where  $\epsilon = \langle \delta V/V_0 \rangle$  is the relative velocity change.

In the stretching algorithm, we multiply the time of the perturbed signal with a stretching factor  $(1 - \epsilon)$  and interpolate the perturbed signal at this stretched time. The time window we use in all our analysis is given by the black bold line in Figure 3. We then stretch the perturbed signal at a regular interval of  $\epsilon$  values. The range of the  $\epsilon$  values can be arbitrarily defined or predicted by prior information on the range of changes in the subsurface velocity.

To resolve the value of  $\epsilon$ , we use an  $L_2$  objective function rather than the cross-correlation algorithm as suggested by *Hadziioannou et al.* [2009]. For events of equal magnitude ( $A = \hat{A}$ ), the objective function is

$$R(\epsilon) = \|\hat{U}(t(1 - \epsilon)) - U(t)\|_2, \quad (13)$$

where  $\|\dots\|_2$  is the  $L_2$  norm. Figure 4 shows the objective function based on the  $L_2$  norm and the maximum cross correlation for the case of a 0.4% velocity change. The  $L_2$  norm more accurately constrains the velocity change than the maximum cross correlation. The minimum of the objective function based on the  $L_2$  norm depends on the amplitude changes between the two signals and on the traveltime perturbations due to velocity changes and shifts in the source location. The signals have uniform magnitudes. The amplitude changes between the signals are due to changes in the orientation of the source angles.

[11] The error in the estimated relative velocity change  $\sigma_{\delta v}$  is given by

$$\sigma_{\delta v} \leq \frac{\sigma_U}{2\pi f_d A t}, \quad (14)$$

where  $f_d$  is the dominant frequency,  $t$  is the centertime of the signal,  $A$  is the amplitude of the signals, and  $\sigma_U$  is the standard deviation of the recorded waveforms. The derivation of equation (14) is given in section C. The error associated with the velocity change depends on additive noise in the signals and on differences in the signals both in amplitude and in phase due to perturbation in source properties.

### 3.3. Effect of Perturbation of Source Properties on the Estimated Velocity Change

[12] To understand the effect of the changes in the source properties on the estimation of the relative velocity changes, we conduct our numerical experiment over a range of parameter changes. We perturb the source location and the orientation of the source angles. The perturbation of the source radiation parameters is characterized by the weighted root mean square change in source parameters ( $r$ ) [*Robinson et al., 2007*]:

$$\langle \zeta \rangle = -\frac{1}{2}(4\Delta\phi^2 + \Delta\lambda^2 + \Delta\delta^2), \quad (15)$$

**Table 1.** Modeling Parameters for Shift in the Source Location

Case	$\frac{\Delta V}{V}$ (%)	$D/\lambda_d$
Reference	0	0
Case 1	0.1	0.0274
Case 2	0.1	0.0547
Case 3	0.1	0.0820
Case 4	0.1	0.1094
Case 5	0.1	0.1367
Case 6	0.1	0.1642
Case 7	0.1	0.1918
Case 8	0.1	0.2197
Case 9	0.1	0.2477
Case 10	0.1	0.2760
Case 11	0.1	0.3047
Case 12	0.1	0.3337
Case 13	0.1	0.3627
Case 14	0.1	0.3916
Case 15	0.1	0.4202

**Table 2.** Modeling Parameters for Source Radiation Perturbation

Case	$\frac{\Delta V}{V}$	$\Delta\phi(^{\circ})$	$\Delta\lambda(^{\circ})$	$\Delta\delta(^{\circ})$	$-(\zeta)$
Reference	0	0	0	0	0
Case 1	0.1	0	0	0	0
Case 2	0.1	2	2	2	0.0037
Case 3	0.1	4	4	4	0.0146
Case 4	0.1	6	6	6	0.0329
Case 5	0.1	8	8	8	0.0585
Case 6	0.1	10	10	10	0.0914
Case 7	0.1	12	12	12	0.1316
Case 8	0.1	14	14	14	0.1791
Case 9	0.1	16	16	16	0.2339
Case 10	0.1	18	18	18	0.2961
Case 11	0.1	20	20	20	0.3655
Case 12	0.1	22	22	22	0.4423
Case 13	0.1	24	24	24	0.5264
Case 14	0.1	26	26	26	0.6178
Case 15	0.1	28	28	28	0.7165

where  $\Delta\phi$  is the change in strike,  $\Delta\lambda$  is the change in rake, and  $\Delta\delta$  is the change in dip, between the two sources.

[13] Figures 5 and 6 show the estimated velocity changes due to the perturbation of medium velocity and the source properties (location and radiation parameters), respectively. For Figure 5, we generate signals with the following perturbation in the model velocity  $\langle\delta V/V_0\rangle$ : 0.1%, 0.2%, 0.3%, and 0.4%. In these models, we keep the source parameters unchanged. Using the stretching method, we are able to recover the velocity changes we impose in the model from the codas of each of the perturbed signals and that of the reference signal (Figure 5). The method accurately estimates the model velocity change in all the receivers. We also generate signals with perturbations in the source locations and mechanisms only. In this case, the true velocity change is zero. Figure 6 shows that the estimated relative velocity changes  $\langle\delta V/V_0\rangle$  are near the true value ( $\delta V = 0$ ) for models with perturbations of either the source location or the source radiation parameters. The velocity change estimated from individual stations varies around zero, but with a shift in the source location of  $D = 0.143\lambda_d$ , with  $\lambda_d$  as the dominant wavelength and source angle perturbations as large as  $\Delta\phi = 20^{\circ}$ ,  $\Delta\lambda = 20^{\circ}$ , and  $\Delta\delta = 20^{\circ}$  ( $\langle\zeta\rangle = -0.366$ ), the magnitude of the estimated velocity change is smaller than 1/20th of the typical velocity changes inferred from seismic signals (Figure 6). These variations in the velocity change inferred from different stations can be used to estimate the errors in the estimated velocity change. These results agree with equation (7) which predicts that the average value of time shifts in the perturbed signal results only from changes in the medium velocity and is not affected by changes in source properties. We will need to know how effectively we can resolve the velocity changes in our model in the presence of the other model parameter perturbations.

### 3.4. Limiting Regimes of the Estimations

[14] To investigate the extent of the perturbation in the source location and source radiation perturbations that can be allowed in the estimation of relative velocity changes, we generate synthetic signals with models having a 0.1% relative velocity change and various perturbations of the source parameters. The values of the source parameter perturbations are given in Tables 1 and 2. Figure 7 shows the

estimated relative velocity changes from signals generated from sources at different locations. The figure shows that we can recover the relative velocity change of 0.1% using doublets (two sources) within a sphere of radius  $\lambda_d/4$ , where  $\lambda_d$  is the dominant wavelength of the seismic signal which is approximately 140 m. This is consistent with the criterion we derived in section D, which predicts that for an accurate estimation of the subsurface velocity change, the shift in the source location has to satisfy

$$\frac{D}{\lambda_d} < \sqrt{2} \left| \left\langle \frac{\delta V}{V_0} \right\rangle \right| f_d t, \quad (16)$$

where  $f_d$  is the dominant frequency of the signals,  $\langle\delta V/V_0\rangle$  is the average velocity change in the subsurface, and  $t$  is the centertime of the processed signal. The criterion is derived from a comparison of the phase changes due to velocity changes with those due to shifts in the source location. For the results in Figure 7, our model parameters are  $\langle\delta V/V_0\rangle = 0.1\%$ ,  $t = 10$  s, and  $f_d \simeq 25$  Hz. With these values, the constraint on the source location shift for Figure 7 is

$$\frac{D}{\lambda_d} < 0.35. \quad (17)$$

Figure 7 shows that for  $D/\lambda_d \geq 0.3$ , the estimated velocity change deviates significantly from the real velocity change; this is in agreement with equation (17). The criterion in equation (16) imposes a constraint on the spacing requirements for the source locations of the doublets used for time-lapse velocity change monitoring with microearthquakes. Alternatively, equation (16) gives the magnitude of a velocity change that is resolvable with a given shift in the source

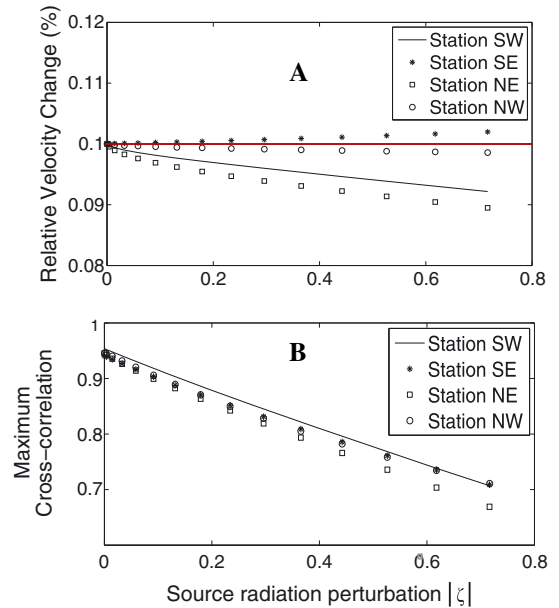


**Figure 8.** Effect of source angle perturbation on estimated velocity change. (a) The estimated relative velocity changes are from a 0.1% model velocity change (red line) and various source radiation perturbations (Table 2). (b) The decorrelation of the doublets, due to source angle perturbations, measured by maximum cross-correlation values. Stations SW, SE, NE, and NW positions are given in Figure 2.

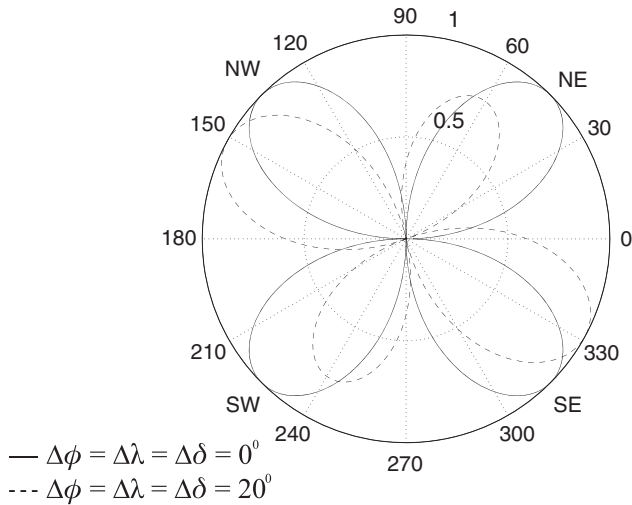


**Figure 9.** Source radiation pattern of the modeled earthquake sources before and after simultaneous perturbation of the source angles (strike  $\Delta\phi$ , rake  $\Delta\lambda$ , and dip  $\Delta\delta$ ) of  $20^\circ$  each.

location. According to equation (16), the allowable source separation increases with the centertime  $t$  of the employed time window. This is due to the fact that the imprint of the velocity change is more pronounced as the waves have propagated over a greater distance through the perturbed medium. However, signals at later times in the coda are more affected by the presence of additive noise because the signal-to-noise ratio usually decreases toward the late coda.

[15] We also investigate the effect of the source radiation properties on the estimated velocity change of the medium of interest. Figure 8 shows the estimated velocity changes from a model with 0.1% velocity change using sources with perturbed radiation angles (measured by  $\langle\zeta\rangle$ ). The values of the perturbed source radiation angles are given in Table 2. In Figure 8a, the estimated velocity change at the individual stations progressively deviates from the true velocity change of 0.1% with increasing change in the orientations of the source angles. This deviation is due to the decorrelation between the perturbed and the unperturbed signals as shown in Figure 8b, which shows the maximum normalized cross correlation of the codas within the processed time window. With an increasing change in the orientation of the sources, the maximum cross-correlation value of the waves excited by the doublets decreases. However, for source angle perturbations as large as  $\Delta\phi = 28^\circ$ ,  $\Delta\lambda = 28^\circ$ , and  $\Delta\delta = 28^\circ$ , which corresponds to  $|\langle\zeta\rangle| = 0.72$  (Figure 8a), the maximum deviation from the 0.1% model velocity change is approximately 0.01%. This is a small change compared to velocity changes resolved from seismic signals in practice. The maximum cross correlation (Figure 8b) can be retrieved from the data and can be used as a diagnostic of the accuracy of the estimated velocity change. In this example, a maximum cross correlation of 0.7 indicates an error of about 10% in the estimated velocity change. The difference in the errors observed among the four stations (SW, SE, NE, and NW) is due to the differences in the amplitude perturbations resulting from the changes in the source angles. Figure 9 shows that with source angle perturbations of  $\Delta\phi = 20^\circ$ ,  $\Delta\lambda = 20^\circ$ ,

and  $\Delta\delta = 20^\circ$ , the loops in the radiation pattern in the NE and SW directions change more dramatically than those in the NW and SE directions. For the parameters used in this experiment, the transport mean free time  $t^*$ , defined as the time over which the scattered waves loses their directions, is given by  $t^* = l^*/c = 8.7$  s.  $c$  is the propagation velocity of the scattered waves. The time interval used for the analysis of the coda waves is 3.6 to 20 s (Figure 3). This means that the coda waves in the early part of the time interval used still retains information about the direction in which they were radiated. The changes in the radiation pattern thereby result to a higher error in velocity changes estimated with stations NE and SW than those with stations NW and SE.

#### 4. Discussion and Conclusion

[16] In this study, we investigate the influence of perturbation in source properties (location and radiation) on the estimation of velocity changes. These velocity changes are extracted from multiply scattered signals (codas) of repeating events. We show that we can resolve accurate values of relative velocity changes if the shift in the source location satisfies equation (16). This constraint depends on the dominant frequency of the signal, the estimated relative velocity change, and the centertime of the employed time window. This places a restriction on the relative event locations that can be used to estimate the relative velocity change of the subsurface. However, to use this constraint, we need to know the magnitude of the relative velocity change we seek to measure. Preliminary results on the velocity change can be used to pick events satisfying equation (16) for an accurate estimation of the velocity changes. Using doublets that do not satisfy the constraint result in an inaccurate estimate of the velocity change. *Weaver et al.* [2011] similarly showed that changes in noise sources induce error in velocity change estimated from correlation signals obtained from the noise signals. Although our study differs from *Weaver et al.* [2011] in that we are using the coda signals from the earthquake sources, the actual velocity changes can be estimated from the signal in the presence of the source perturbation as shown by *Weaver et al.* [2011], except when the criterion in equation (16) is violated.

[17] A significant change in the source mechanism of double-couple sources can introduce a bias in the estimation of relative velocity change. This bias is due to the decorrelation of the perturbed and unperturbed signals which lowers the accuracy of the estimated velocity change. As shown in Figures 6b and 8a, some of the stations underestimate while others overestimate the velocity change. However, this bias is negligible for the typical velocity changes resolved from seismic signals in practice. This result permits the use of sources of different orientations for the estimation of velocity changes, provided that the maximum cross correlation of the source signals is greater than 0.7 as shown in Figure 8b. For a consistent estimate of the velocity change, using multiple stations is useful to ascertain the accuracy of the estimated velocity change in an isotropic subsurface.

[18] The theory presented in this study is based on a number of simplifications and assumptions. First, we assume a uniform velocity change across our model. For the case of a localized isotropic velocity change, the resolved velocity change is a fraction of the local velocity change,

where the fraction is dependent on the amount of time the codas spend within the perturbed region relative to the unperturbed region.

[19] In this study, we assume that the scatterer density is uniform in all directions from the source. We also ignore changes in the scattering properties which might include shifts in scatterer locations [Niu *et al.*, 2003; Snieder and Page, 2007] and changes in the scattering strength of the scatterers. These changes in the scatterer properties can be due to changes in fluid properties such as fluid migration or opening and closing of fractures and pre-existing faults. If the shifts in the scatterer location are random, then the average traveltimes perturbation due to scatterer location shift is zero. However, if the shifts in the scatterer locations are nonrandom or directional, then the average time perturbation due to scatterer location shift over all takeoff angles is a nonzero mean traveltime change. A nonzero mean traveltime perturbation is also expected for nonuniform scatterer density. The scattered signals lag behind while traveling through a higher scatterer density region compared to a lower scatterer density region. These introduce a bias in the estimated relative velocity changes if the changes in scatterer properties or density are significant.

[20] We used point scatterers in our numerical modeling even though in the real world, scattering can be caused by faults, fractures, horizontal, or dipping layers. The employed modeling uses scalar waves; hence, it does not account for mode conversions of elastic waves (for example, *P*-to-*S* or *S*-to-*P* and surface waves) that might result due to the presence of layers, free surface, and fractures. The coda is usually dominated by *S* wave [Aki and Chouet, 1975; Snieder, 2002]; hence, the mode conversions between *P* and *S* waves do not dominate the details of the scattering processes.

### Appendix A: The Time Perturbation Due to a Perturbed Source

[21] From Figure 1, the traveltime  $t_T$  for the signal along path  $T$  from the unperturbed source to the first scatterer along path  $T$  is given by

$$t_T = \frac{L_T}{V_0}, \quad (\text{A1})$$

where  $V_0$  is the unperturbed medium velocity. The traveltime  $t_{T'}$  for the signal along path  $T'$  from the perturbed source to the same first scatterer is given by

$$t_{T'} = \frac{L_{T'}}{V}. \quad (\text{A2})$$

We assume that the signals from both sources after scattering by the first scatterer travel along the same path (Figure 1). We define  $L_T = L_{T'} + \delta L$  and  $V = V_0 + \delta V$ , where  $\delta L = -(\hat{\mathbf{r}}_T \cdot \mathbf{D})$ , with  $\mathbf{D}$  as the perturbation of the source location and  $\hat{\mathbf{r}}_T$  as the takeoff direction from the first source to the scatterer. The takeoff direction from the source  $\hat{\mathbf{r}}_T$  in spherical coordinates is

$$\hat{\mathbf{r}}_T = \begin{pmatrix} \cos \psi \sin \theta \\ \sin \psi \sin \theta \\ \cos \theta \end{pmatrix}, \quad (\text{A3})$$

where  $\theta$  and  $\psi$  are the co-latitude and longitude in spherical coordinates, respectively. The traveltime for the signal along

path  $T$  from the second source to the first scatterer can be re-expressed as

$$t_{T'} = \frac{L_{T'}}{V_0 + \delta V} \quad (\text{A4})$$

$$\simeq \left( \frac{1}{V_0} - \frac{\delta V}{V_0^2} + \dots \right) L_T - \left( \frac{1}{V_0} - \frac{\delta V}{V_0^2} + \dots \right) \cdot (\hat{\mathbf{r}}_T \cdot \mathbf{D}). \quad (\text{A5})$$

Ignoring the terms of second order or higher in the velocity change and source displacement, equation (A5) gives,

$$t_{T'} \simeq \frac{L_T}{V_0} - \left( \frac{\delta V}{V_0} \right) \left( \frac{L_T}{V_0} \right) - \frac{(\hat{\mathbf{r}}_T \cdot \mathbf{D})}{V_0}, \quad (\text{A6})$$

$$= t_T + t_{pv} + t_{pl}. \quad (\text{A7})$$

Therefore, the time perturbation along path  $T'$  is given as

$$t_p^{T'} = t_{T'} - t_T = t_{pv} + t_{pl}, \quad (\text{A8})$$

where  $t_{pv}$  is the time shift due to velocity change and  $t_{pl}$  is the time shift due to shift in source.

[22] We need to derive the expression for  $\langle t_p \rangle$ . With equations (6) and (A8), the average time perturbation is given,

$$\begin{aligned} \langle t_p \rangle &= \frac{\sum_T A_T^2 t_p^{T'}}{\sum_T A_T^2} = \frac{-\sum_T A_T^2 \left( \left( \frac{\delta V}{V_0} \right) \left( \frac{L_T}{V_0} \right) + \left( \frac{\hat{\mathbf{r}}_T \cdot \mathbf{D}}{V_0} \right) \right)}{\sum_T A_T^2}, \\ &= \left\langle \frac{\delta V}{V_0} \right\rangle \frac{\int_T L_T / V_0 d\Omega}{\int_T d\Omega} + \frac{\int_T (\hat{\mathbf{r}}_T \cdot \mathbf{D}) / V_0 d\Omega}{\int_T d\Omega}, \end{aligned} \quad (\text{A9})$$

where  $\int_T \dots d\Omega$  denotes an integration over all takeoff angles. In 3-D, the integration limits of  $d\theta$  and  $d\psi$  are  $[0, \pi]$  and  $[0, 2\pi]$ , respectively. Since  $\int_T \hat{\mathbf{r}}_T d\Omega = 0$  and  $\int_T (L_T / V_0) d\Omega / \int_T d\Omega = t$ , where  $t$  is the traveltime of the scattered ray from the source to the receiver along path  $T$ , equation (A9) reduces to

$$\langle t_p \rangle = - \left\langle \frac{\delta V}{V_0} \right\rangle t. \quad (\text{A10})$$

Hence, to first order in  $\mathbf{D}$ , the average traveltime perturbation depends only on the velocity changes within the explored medium.

### Appendix B: Variance of Time Perturbation

[23] The variance of the traveltime perturbation, using equation (6), is given by

$$\sigma_t^2 = \frac{\sum_T A_T^2 (t_p - \langle t_p \rangle)^2}{\sum_T A_T^2} = \langle t_p^2 \rangle - \langle t_p \rangle^2, \quad (\text{B1})$$

where using expression (A8)  $\langle t_p^2 \rangle$  is given by

$$\langle t_p^2 \rangle = \frac{\sum_T A_T^2 \left( - \left( \frac{\delta V}{V_0} \right) \left( \frac{L_T}{V_0} \right) - \frac{\hat{\mathbf{r}}_T \cdot \mathbf{D}}{V_0} \right)^2}{\sum_T A_T^2}. \quad (\text{B2})$$

Expanding equation (B2) gives

$$\begin{aligned} \langle t_p^2 \rangle &= \sum_T A_T^2 \left( \left( \frac{\delta V}{V_0} \right)^2 \left( \frac{L_T}{V_0} \right)^2 + \left( \frac{\hat{\mathbf{r}}_T \cdot \mathbf{D}}{V_0} \right)^2 \right. \\ &\quad \left. + 2 \left( \frac{\delta V}{V_0} \right) \left( \frac{L_T}{V_0} \right) \left( \frac{\hat{\mathbf{r}}_T \cdot \mathbf{D}}{V_0} \right) \right) / \sum_T A_T^2. \end{aligned} \quad (\text{B3})$$

In equation (B3),

$$\frac{\int_T (\hat{\mathbf{r}}_T \cdot \mathbf{D})^2 d\Omega}{\int_T d\Omega} = \frac{D^2}{C}, \quad (\text{B4})$$

where  $C = 1, 2,$  or  $3$  equals the dimension of the problem and

$$\frac{\int_T \hat{\mathbf{r}}_T \cdot \mathbf{D} d\Omega}{\int_T d\Omega} = 0, \quad (\text{B5})$$

Therefore, in 3-D,

$$\langle t_p^2 \rangle = \left\langle \frac{\delta V}{V_0} \right\rangle^2 t^2 + \frac{D^2}{3V_0^2}, \quad (\text{B6})$$

Combining equations (B5) and (A10), the total variance of the time perturbation is

$$\sigma_t^2 = \frac{D^2}{3V_0^2}. \quad (\text{B7})$$

In the absence of additive noise, the variance of the travel-time perturbation thus depends only on the shift in the source location. With the estimate of the subsurface velocity, we can estimate the shift in the source location from equation (B7).

### Appendix C: Error Estimation

[24] We estimate the error associated with the estimated relative velocity change using the data residuals from the  $L_2$  norm. Using equation (7) and a Taylor series expansion of  $\hat{U}(t + t_p)$  with respect to  $t$  in terms of  $U(t)$ ,

$$\hat{U}(t + t_p) = \hat{U}(t - \epsilon t) \simeq U(t) - \epsilon t \frac{dU(t)}{dt}, \quad (\text{C1})$$

where  $\epsilon = \left\langle \frac{\delta V}{V_0} \right\rangle$ . Here, we assume that  $\epsilon$  is constant across the signal. Including additive errors  $\delta U(t)$  in the data with standard deviation  $\sigma_U$ , equation (C1) gives

$$\hat{U}(t - \epsilon t) + \delta U(t) \simeq U(t) - (\epsilon + \delta\epsilon) t \frac{dU}{dt}, \quad (\text{C2})$$

where  $\delta\epsilon$  is the error of the relative velocity change due to the error in the data  $\hat{U}(t + t_p)$ . The relationship between the data error and the error in the relative velocity change, then gives

$$\sigma_U \simeq \sigma_{\delta v} t \frac{dU}{dt}, \quad (\text{C3})$$

where  $\sigma_{\delta v}$  is the standard deviation of the error in the relative velocity change. Therefore, the error in the relative velocity change between the perturbed and unperturbed signals is

$$\sigma_{\delta v} = \|\hat{\epsilon} - \epsilon\|_2 \leq \frac{\sigma_U}{\|M\|_2}, \quad (\text{C4})$$

where  $\hat{\epsilon}$  and  $\epsilon$  are the estimated and the exact relative velocity changes, respectively, and  $\|M\|_2$  is  $2\pi f_d t \|U\|_2$ , with  $f_d$  as the dominant frequency of the signal. Therefore, the error in the estimated relative velocity change  $\sigma_{\delta v}$  is

$$\sigma_{\delta v} \leq \frac{\sigma_U}{\|U\|_2 2\pi f_d t}. \quad (\text{C5})$$

In practice,  $t$  is the centertime of the used time window, and  $\|U\|_2$  is the amplitude of the data.

[25] The error equation (equation (C5)) depends on the dominant frequency of the signal, the length of the signals,

and the amplitude difference between the signals  $\hat{U}(t)$  and  $U(t)$  which is normalized by the amplitude of  $U(t)$ . The error in the data  $\sigma_U$  is due to any dissimilarity between the two signals  $\hat{U}(t)$  and  $U(t)$  resulting from either shift in the source location or the presence of additive noise.

### Appendix D: Comparative Time Shift Between Changes in Velocity and Source Location

[26] In this section, we compare phase shifts due to the shift in the source location to the phase shifts resulting from velocity change within the subsurface. If the phase of the wave that travels over a distance  $r$  from a source to a scatterer is  $\exp(i\mathbf{k} \cdot \mathbf{r}_T)$ , then the phase change due to shift in the source location along path  $T$  is

$$\exp(-ik(\hat{\mathbf{r}}_T \cdot \mathbf{D})) = \exp(-ikD \cos \theta_T), \quad (\text{D1})$$

where  $\theta_T$  is the angle between the takeoff ray of path  $T$  and the shift in the source location  $D$ , and  $k = 2\pi/\lambda$ . For  $D/\lambda < 1$ , we can approximate equation (D1) as

$$\exp(-ikD \cos \theta_T) \simeq 1 - ikD \cos \theta_T - \frac{1}{2}(kD \cos \theta_T)^2. \quad (\text{D2})$$

The average value of the phase changes due to the shift in the source location is

$$\langle \exp(-ikD \cos \theta_T) \rangle \simeq 1 - ikD \langle \cos \theta_T \rangle - \frac{1}{2}(kD)^2 \langle \cos^2 \theta_T \rangle, \quad (\text{D3})$$

assuming we sum over all angles  $\langle \cos \theta_T \rangle = 0$ . For equal contribution from all takeoff angles in 2-D (the numerical simulations in section 3 are in 2-D),  $\langle \cos^2 \theta_T \rangle = \frac{1}{2}$ . Therefore,

$$\langle \exp(-ikD \cos \theta_T) \rangle \simeq 1 - \frac{1}{4}k^2 D^2. \quad (\text{D4})$$

Also, if the phase of the wave that travels over a time  $t$  is  $\exp(-i\omega t)$ , then the phase change due to the change in the medium velocity is

$$\exp(-i\omega \Delta t) \simeq 1 - i\omega \Delta t - \frac{1}{2}(\omega \Delta t)^2, \quad (\text{D5})$$

where  $\Delta t$  is the time shift due to velocity change. The second-order terms contribute to the variance of the phase change. Therefore, for an accurate estimation of the velocity change,

$$\frac{1}{4}k^2 D^2 < \frac{1}{2}\omega^2 \Delta t^2. \quad (\text{D6})$$

Equation (D6) implies that

$$\frac{D}{\lambda} < \sqrt{2} f |\Delta t|. \quad (\text{D7})$$

But the average value of time shift due to velocity change  $\langle \Delta t \rangle$  is

$$\langle \Delta t \rangle = - \left\langle \frac{\delta V}{V_0} \right\rangle t. \quad (\text{D8})$$

Therefore, equation (D7) reduces to

$$\frac{D}{\lambda} < \sqrt{2} f \left| \left\langle \frac{\delta V}{V_0} \right\rangle \right| t. \quad (\text{D9})$$

Equation (D9) shows that for an accurate estimation of relative velocity changes, the shift in the source location  $D$  has to satisfy equation (D9). For practical purposes,  $\lambda$  and  $f$  can

be defined as the dominant wavelength and frequency of the processed signal, respectively. Also,  $t$  can be assigned as the centertime of the used time window.

[27] **Acknowledgments.** We thank two anonymous reviewers for the critical and constructive comments. This work was supported by the U.S. Department of Energy through grant DE-EE0002758.

## References

- Aki, K., and L. Chouet (1975), Origin of coda waves: Source, attenuation, and scattering effects, *J. Geophys. Res.*, *80*, 3322–3342.
- Aki, K., and P. G. Richards (2002), *Quantitative Seismology*, pp. 101–113, University Science Books, Sausalito, Calif.
- Asano, Y., T. Saito, Y. Ito, K. Shiomi, H. Hirose, T. Matsumoto, S. Aoi, S. Hori, and S. Sekiguchi (2011), Spatial distribution and focal mechanisms of aftershocks of the 2011 off the Pacific coast of Tohoku Earthquake, *Earth Planets Space*, *63*(7), 669–673, doi:10.5047/eps.2011.06.016.
- Brenguier, F., M. Campillo, C. Hadziioannou, N. Shapiro, and E. Larose (2008), Postseismic relaxation along the San Andreas Fault at Parkfield from continuous seismological observations, *Science*, *321*, 1478–1481.
- Busch, K., C. M. Soukoulis, and E. N. Economou (1994), Transport and scattering mean free paths of classical waves, *Phys. Rev. B*, *50*(1), 93–98, doi:10.1103/PhysRevB.50.93.
- Cheng, X., F. Niu, and B. Wang (2010), Coseismic velocity change in the rupture zone of the 2008 Mw 7.9 Wenchuan earthquake observed from ambient seismic noise, *Bull. Seismol. Soc. Am.*, *100*(5B), 2539–2550, doi:10.1785/0120090329.
- Davis, T. L., M. J. Terrell, R. D. Benson, R. Cardona, R. R. Kendall, and R. Winarsky (2003), Multicomponent seismic characterization and monitoring of the CO<sub>2</sub> flood at Weyburn Field, Saskatchewan, *The Leading Edge*, *22*(7), 696–697, doi:10.1190/1.1599699.
- Foldy, L. L. (1945), The multiple scattering of waves. I. General theory of isotropic scattering by randomly distributed scatterers, *Phys. Rev.*, *67*(3-4), 107–119, doi:10.1103/PhysRev.67.107.
- Godano, M., T. Bardainne, M. Regnier, A. Deschamps, and M. Valette (2012), Spatial and temporal evolution of a microseismic swarm induced by water injection in the ArkemaVauvert salt field (Southern France), *Geophys. J. Int.*, *188*(1), 274–292, doi:10.1111/j.1365-246X.2011.05257.x.
- Groenenboom, J., and R. Snieder (1995), Attenuation, dispersion, and anisotropy by multiple scattering of transmitted waves through distributions of scatterers, *J. Acoust. Soc. Am.*, *98*(6), 3482–3492, doi:10.1121/1.413780.
- Hadziioannou, C., E. Larose, O. Coutant, P. Roux, and M. Campillo (2009), Stability of monitoring weak changes in multiply scattering media with ambient noise correlation: Laboratory experiments, *J. Acoust. Soc. Am.*, *125*(6), 3688–3695, doi:10.1121/1.3125345.
- Lipman, P., J. Lockwood, R. Okamura, D. Swanson, and K. Yamashita (1985), Ground deformation associated with the 1975 magnitude-7.2 earthquake and resulting changes in activity of Kilauea volcano, Hawaii, *U.S. Geol. Surv. Prof. Pap.*, *1276*, 45.
- McGuire, J. J., J. A. Collins, P. Goudard, E. Roland, D. Lizarralde, M. S. Boettcher, M. D. Behn, and R. D. van der Hilst (2012), Variations in earthquake rupture properties along the Gofar transform fault, East Pacific Rise, *Nat. Geosci.*, *5*(5), 336–341, doi:10.1038/ngeo1454.
- Meier, U., S. N. M., and F. Brenguier (2010), Detecting seasonal variations in seismic velocities within Los Angeles basin from correlations of ambient seismic noise, *Geophys. J. Int.*, *181*, 985–996.
- Miyazawa, M., A. Venkataraman, R. Snieder, and M. A. Payne (2007), Analysis of microearthquake data at cold lake and its applications to reservoir monitoring, *SEG Tech. Program Expanded Abstr.*, *26*(1), 1266–1270, doi:10.1190/1.2792734.
- Niu, F., P. Silver, R. Nadeau, and T. McEvilly (2003), Migration of seismic scatterers associated with the 1993 Parkfield aseismic transient event, *Nature*, *426*, 544–548.
- Poupinet, G., W. L. Ellsworth, and J. Frechet (1984), Monitoring velocity variations in the crust using earthquake doublets: An application to the Calaveras fault, California, *J. Geophys. Res.*, *89*(B7), 5719–5731, doi:10.1029/JB089iB07p05719.
- Robinson, D. J., R. Snieder, and M. Sambridge (2007), Using coda wave interferometry for estimating the variation in source mechanism between double couple events, *J. Geophys. Res.*, *112*, B12302, doi:10.1029/2007JB004925.
- Robinson, D. J., M. Sambridge, and R. Snieder (2011), A probabilistic approach for estimating the separation between a pair of earthquakes directly from their coda waves, *J. Geophys. Res.*, *116*, B04309, doi:10.1029/2010JB007745.
- Sasaki, S., and H. Kaieda (2002), Determination of stress state from focal mechanisms of microseismic events induced during hydraulic injection at the Hijiori hot dry rock site, *Pure Appl. Geophys.*, *159*(1), 489–516, doi:10.1007/PL00001262.
- Sens-Schönfelder, C., and U. Wegler (2006), Passive image interferometry and seasonal variations at Merapi volcano, Indonesia, *Geophys. Res. Lett.*, *33*, L21302, doi:10.1029/2006GL027797.
- Snieder, R. (2002), Coda wave interferometry and the equilibration of energy in elastic media, *Phys. Rev. E*, *66*(4), 046615, doi:10.1103/PhysRevE.66.046615.
- Snieder, R. (2006), The theory of coda wave interferometry, *Pure Appl. Geophys.*, *163*(2-3), 455–473, doi:10.1007/s00024-005-0026-6.
- Snieder, R., and J. Page (2007), Multiple scattering in evolving media, *Phys. Today*, *60*(5), 49–55, doi:10.1063/1.2743124.
- Snieder, R., and M. Vrijlandt (2005), Constraining the source separation with coda wave interferometry: Theory and application to earthquake doublets in the Hayward fault, California, *J. Geophys. Res.*, *110*, B04301, doi:10.1029/2004JB003317.
- Snieder, R., A. Grêt, H. Douma, and J. Scales (2002), Coda wave interferometry for estimating nonlinear behavior in seismic velocity, *Science*, *295*(5563), 2253–2255.
- Vesnaver, A. L., F. Accaino, G. Bohm, G. Madrussani, J. Pajchel, G. Rossi, and G. D. Moro (2003), Time-lapse tomography, *Geophysics*, *68*(3), 815–823, doi:10.1126/science.1070015.
- Weaver, R. L., C. Hadziioannou, E. Larose, and M. Campillo (2011), On the precision of noise correlation interferometry, *Geophys. J. Int.*, *185*(3), 1384–1392, doi:10.1190/1.1581034.
- Wegler, U., and C. Sens-Schönfelder (2007), Fault zone monitoring with passive image interferometry, *Geophys. J. Int.*, *168*, 1029–1033, doi:10.1111/j.1365-246X.2011.05015.x.
- Zoback, M., and J. Zinke (2002), Production-induced normal faulting in the Valhall and Ekofisk oil fields, *Pure Appl. Geophys.*, *159*(1), 403–420, doi:10.1007/PL00001258.
- Zoback, M. D., and H. Harjes (1997), Injection-induced earthquakes and crustal stress at 9 km depth at the KTB deep drilling site, Germany, *J. Geophys. Res.*, *102*(B8), 18,477–18,491, doi:10.1029/96JB02814.